227 (2023) 211825

Contents lists available at ScienceDirect

Geoenergy Science and Engineering

journal homepage: www.sciencedirect.com/journal/geoenergy-science-and-engineering

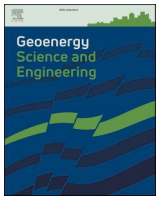

Analytical solutions for the injection of wettability modifiers in carbonate reservoirs based on a reduced surface complexation model

Ricardo A. Lara Orozco, Ryosuke Okuno *, Larry W. Lake

The Hildebrand Department of Petroleum and Geosystems Engineering, The University of Texas at Austin, Austin, TX, USA

ARTICLE INFO

Keywords:
Wettability alteration
Sulfate
Glycine
Surface complexation modeling
Method of characteristics
Carbonate reservoirs

ABSTRACT

The potential of tuned-composition waterflooding to enhance oil recovery from carbonate reservoirs has been widely investigated, where wettability alteration is the dominant mechanism. It is hypothesized that the sulfate in seawater adsorbs on the rock surface, removing acidic hydrocarbon species adsorbed thereon. Glycine, the simplest amino acid, has also been investigated as a wettability modifier for carbonates that acts similarly to sulfate.

Wettability alteration by the adsorption of sulfate ion and glycine anion has been satisfactorily modeled by extending calcite's surface complexation model (SCM) based on zeta potential measurements. However, determining the relevance of the individual geochemical reactions is obscured by the complexity of the SCM. Moreover, the large number of equilibrium constants and their associated uncertainty result in many degrees of freedom when matching corefloods and spontaneous imbibition experiments.

This research determines the chemical reactions in the calcite's SCM that govern wettability alteration and the incremental oil recovery by glycine-enhanced waterflooding in carbonate reservoirs. We found that the wettability alteration by SCM can be approximated by two anion exchange reactions between the wettability modifiers, sulfate and glycine anions, and the carboxylic acids adsorbed on the rock surface. Moreover, the wettability of the system described by the adsorption of carboxylic acids and the incremental oil recovery by waterflooding are linearly correlated with the K value of the reaction of carboxylic acids with the carbonate surface and the concentration of carboxylic acids in the system, which is a function of the total acid number.

We present analytical solutions for the two-phase, multicomponent reactive-transport model coupled with anion exchange reactions. To the best of our knowledge, this is the first time the presented analytical solutions are applied to describe enhanced waterflooding in carbonate reservoirs where more than one wettability modifier is injected. The analytical solutions showed that glycine injection enhances oil recovery over waterflooding by the formation of two wettability alteration waves. The number of waves and their types (rarefaction or shock) depend on glycine's and sulfate's concentration at the injection. The improvement in oil recovery by wettability alteration mainly occurs because the more favorable mobility ratio increases the displacement efficiency with no reduction in residual oil saturation. A synergy was found between glycine and sulfate, where the presence of glycine promotes the formation of a wettability-alteration shock by sulfate that improves the displacement efficiency.

CRediT author statement

Ricardo A. Lara Orozco: Data curation; Formal analysis; Investigation; Methodology; Validation; Visualization; Writing – original draft. Ryosuke Okuno: Conceptualization; Formal analysis; Funding acquisition; Investigation; Methodology; Project administration; Resources; Supervision; Validation; Writing – review & editing. Larry W. Lake: Conceptualization; Formal analysis; Investigation; Methodology; Supervision; Validation; Writing – review & editing.

1. Introduction

Carbonate reservoirs contain over 50% of the world's oil reserves (Akbar et al., 2000). However, the recovery factor after waterflooding is small (around 26% of the oil originally in place) because carbonates are commonly naturally fractured and the oil-wetting nature of the rock

* Corresponding author.
E-mail addresses: rlara@utexas.edu (R.A. Lara Orozco), okuno@utexas.edu (R. Okuno), larry_lake@mail.utexas.edu (L.W. Lake).

https://doi.org/10.1016/j.geoen.2023.211825
Received 12 September 2022; Received in revised form 16 February 2023; Accepted 18 April 2023
Available online 29 April 2023

matrix prevents the imbibition of the injection brine (Allan and Sun, 2003). Therefore, research on chemically enhanced oil recovery for carbonate reservoirs is of great interest, given their economic importance and the low capital investment required for existing-waterflooded mature fields (Manrique et al., 2007). Examples of chemical EOR applied to carbonates include polymer (Al-Sofi et al., 2019), surfactants (Moradi et al. (2019), and alkaline flooding (Abu-Al-Saud et al., 2020). The injected chemicals, however, need to withstand the high temperatures and the high salinity brines typically found in carbonate reservoirs.

Low-salinity waterflooding (LSW) consists of injecting brine that has a smaller ionic strength and/or a larger sulfate concentration than the formation brine. Its application to enhance oil recovery in carbonate reservoirs has been extensively investigated in the past two decades, having the advantages of being a low-cost, simple-to-implement EOR method. There is a consensus that wettability alteration is responsible for the incremental oil recovery observed in laboratory experiments (Yousef et al., 2011; Zhang et al., 2007) and field-scale applications; however, the underlying mechanisms are still debated. The mechanisms that have been proposed for this recovery include calcite dissolution (Hiorth et al., 2010), expansion of the electric double layer (Hirasaki, 1991), and multicomponent ion exchange (Zhang et al. 2017). The latter mechanism is the basis of this study.

The combination of LSW and other chemical EOR techniques, known as hybrid methods, has been investigated in recent years. For instance, combining LSW/surfactant flooding (Sekerbayeva et al., 2022; Shakeel et al., 2021), LSW/polymer flooding (Brantson et al., 2020; Karimov et al., 2020), and LSW/nanoparticles (Ebrahim et al., 2019). The motivation is to improve oil recovery by the combination of mechanisms, such as IFT reduction, wettability alteration, and mobility control. Given that there is no technology to selectively reduce the concentration of ions in brines, along with the operational hurdles, e.g., reservoir souring and bacterial growth, related to the high concentration of sulfates, investigating hybrid methods with LSW is an ongoing research topic (Gbadamosi et al., 2022).

Glycine, the simplest amino acid, has been recently investigated to improve LSW in carbonate reservoirs (Lara Orozco et al., 2020a,b). It has the advantages of being a non-toxic, environmentally friendly chemical that is commercially available at a low cost (Tripathi and Mohanty, 2008). Its potential as a wettability modifier was shown in contact angle measurements and spontaneous imbibition experiments performed at 95 °C. A solution of formation brine with 5 wt% glycine significantly decreased the contact angle of oil droplets placed on oil-wet, synthetic calcite pieces. Spontaneous imbibition experiments with Indiana limestone cores showed that the solutions with 5 wt% glycine in formation brine, seawater, and LSW, increased oil recovery by 25% of the mobile oil compared to LSW. The working hypothesis of the wettability alteration mechanism is the electrostatic interaction between glycine anion and the positively charged carbonate surface. This was confirmed from zeta potential measurements of synthetic calcite particles (Lara Orozco et al., 2021b), where the addition of glycine resulted in the decrease of the zeta potential.

Multicomponent ion exchange has been proposed as the main underlying mechanism behind wettability alteration by LSW. It involves the adsorption of potential determining ions (PDIs), Ca^{2+}, Mg^{2+}, and SO_4^{-2} that causes the desorption of oil. Surface complexation modeling has been successfully used to describe the adsorption of PDIs onto carbonate surfaces, capturing the trends observed in laboratory measurements, such as zeta potential and contact angle measurements. One approach to modeling wettability alteration is SCM with the addition of a surface complexation reaction that models the adsorption of carboxylic acids\. Based on the mechanism of wettability alteration by sulfate ions in LSW, Lara Orozco et al. (2021a) proposed a surface complexation reaction that describes glycine adsorption onto the carbonate surface based on the aqueous complexation between glycine and calcium ions. The intrinsic equilibrium constant was tuned with zeta potential measurements of synthetic calcite particles in brines with varying ionic compositions and glycine concentrations (Lara Orozco et al., 2021b). The change in adsorbed carboxylic acids calculated by the SCM followed the trends of lower contact angle and higher oil recovery in spontaneous imbibition experiments with glycine solutions.

SCMs can be used with reservoir simulators to investigate the enhancement of oil recovery by wettability alteration. The amount of adsorbed carboxylic acids calculated by the SCMs is used as an indicator of the rock wettability to linearly interpolate between two sets of relative permeabilities that represent the most water- and oil-wetting states of the system. This approach was followed in many studies of LSW in carbonates, e.g., Qiao et al. (2016), Eftekhari et al. (2017), Sharma and Mohanty (2018), and Sharma and Mohanty (2022). Simulation studies of LSW help investigate design parameters, such as seawater slug size, injected water salinity, and optimum ionic composition. However, the large number of aqueous and surface complexation reactions can complicate the interpretation of the results. In contrast, analytical solutions facilitate the interpretation of laboratory core floods, serve as a validation tool for numerical simulators, and yield a deep understanding of the underlying mechanisms and transport behavior. This motivates ongoing research on deriving exact solutions to both secondary and tertiary recovery methods, (Lake et al., 2014, Ding et al. 2020; Chengjun et al. 2022), e.g., gas (Khorsandi et al., 2016), foam (Zanganesh 2011), polymer (Borazjani et al., 2020; Apolinário and Pires, 2021), and waterflooding in fractured reservoirs (Velasco-Lozano and Balhoff, 2021).

Various analytical studies on wettability alteration by LSW are in the literature. Tripathi and Mohanty (2008) presented an analytical solution based on fractional flow theory for 1D tertiary LSW to study flow instabilities caused by wettability alteration. Al–Ibadi et al. (2019) extended this model to consider the impact of salinity dispersion. In both studies, the impact of brine composition on wettability alteration is neglected, and it is instead modeled as a function of brine salinity. Awolayo and Sarma (2019) studied the effect of injected brine chemistry on the wettability alteration of carbonate rocks. The study considered, however, only single-phase flow modeling the transport and adsorption of SO_4^{2-}, Ca^{2+}, and Mg^{2+}. Taheriotaghsara et al. (2020) presented an analytical solution of two-phase flow with ion adsorption to study wettability alteration by LSW in carbonates. The adsorption of Ca^{2+}, Mg^{2+}, and SO_4^{2-} was modeled by Langmuir isotherms fitted to a calcite SCM. Wettability was considered to be a function of the concentration of adsorbed ions. The analytical model was able to match the oil recovery and pressure drop history of several LSW core floods. The best fit was obtained when wettability alteration was a function of the adsorption of Ca^{2+}. The proposed model, however, assumes that the adsorption of a single component only depends on its own concentration and neglects the impact of the other components present in the system. Khorsandi et al. (2017) presented analytical solution of two-phase multicomponent transport to study the synergy of LSW and polymer flooding in sandstone reservoirs. The adsorption Ca^{2+}, Mg^{2+}, and Na^{+} was modeled as cation exchange reactions, and wettability alteration was defined as a function of adsorbed Na^{+}. The solutions were compared with numerical solutions and experimental results.

The objective of this research is to investigate the impact of the transport of glycine anion and sulfate anion on enhance oil recovery during waterflooding in carbonates. The main novelty in this research is the reduction of calcite's surface complexation model into a set of anion exchange reactions between wettability modifiers and carboxylic acids adsorbed on the rock surface. The main difference between this research and Taheriotaghsara et al. (2020) is that we consider anion exchange reactions to explicitly model the desorption of carboxylic acids by the presence of wettability modifiers. Taheriotaghsara et al. (2020) used Langmuir isotherms to model the adsorption of Ca^{2+}, Mg^{2+}, and SO_4^{2-}. The adsorption of an ion only depended on its own concentration, e.g., the adsorption of Ca^{2+} did not depend on the concentration of Mg^{2+}. The

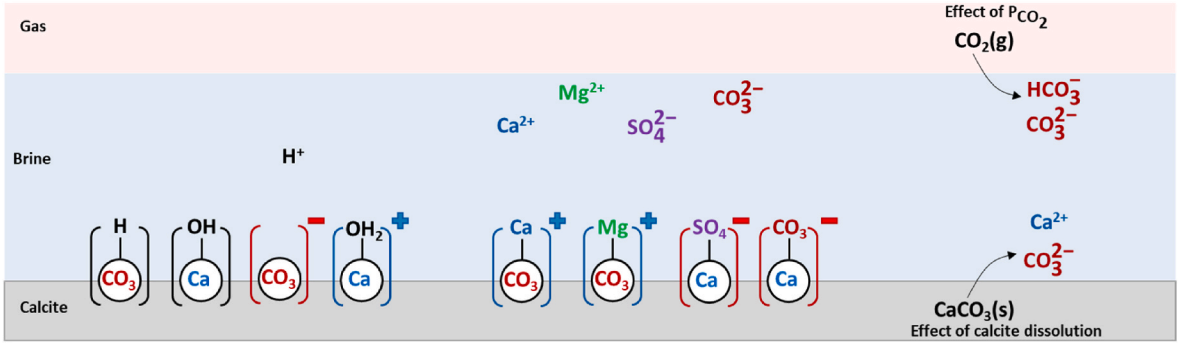

Fig. 1. Schematic of surface complexation reaction to model the adsorption of ions in the brine. Additional chemical reactions can be considered like calcite dissolution and the solubilization of carbon dioxide.

Table 1
Surface complexation reactions considered in the numerical model of single-phase displacements.

No	Surface complexation reaction					log K (25 °C)
S1	$>CaOH_2^+$			$\Longleftrightarrow$	$>CaOH$	+ H^+ −11.85
S2	$>CaOH_2^+$	+	SO_4^{2-}	$\Longleftrightarrow$	$>CaSO_4^-$	+ H_2O 2.10
S3	$>CaOH_2^+$	+	CO_3^{2-}	$\Longleftrightarrow$	$>CaCO_3^-$	+ H_2O 4.53
S4	$>CO_3^-$	+	H^+	$\Longleftrightarrow$	$>CO_3H$	5.10
S5	$>CO_3^-$	+	Ca^{2+}	$\Longleftrightarrow$	$>CO_3Ca^+$	2.50
S6	$>CO_3$	+	Mg^{2+}	$\Longleftrightarrow$	$>CO_3Mg^+$	2.50
S7	$>CaOH_2^+$	+	Gly^-	$\Longleftrightarrow$	$>CaGly$	+ H_2O 1.93
S8	$>CaOH_2^+$	+	$-COO^-$	$\Longleftrightarrow$	$>CaOH_2COO$	−1.51

Table 2
Aqueous reactions describing the speciation of glycine as a function of the solution pH. The equilibrium constants at 95 °C were calculated using the van't Hoff equation proposed in Clarke et al. (2005).

	Reaction							log K (25 °C)	log K (95 °C)
Aqueous speciation									
G1	GlyH	+	H^+	$\Longleftrightarrow$	$GlyH_2^+$			2.34	2.32
G2	GlyH			$\Longleftrightarrow$	Gly^-	+	H^+	−9.78	−8.34

proposed model in this research can be solved by transforming the two-phase flow and reactive-transport problems into Lagrangian coordinates to decouple them. They are then solved using the method of characteristics following Pires et al. (2006), Venkatraman et al. (2014), and Khorsandi et al. (2017).

2. Method

2.1. Calcite's surface complexation model

A SCM describes the chemical and electrostatic interactions between ions in the solution and the rock's surface. The SCM for calcite considers two main surface sites, $>CaOH$, and $>CO_3H$. These sites can be protonated or deprotonated depending on the solution pH to form the charged surface species $>CaOH_2^+$ and $>CO_3^-$. The ions in the brine can also adsorb on the rock surface to form charged surface species (Fig. 1). The adsorption of ions is described by mass action equations where the intrinsic equilibrium constant K is corrected by considering the electrostatic interactions between the ions and the rock surface (Van Cappellen et al., 1993):

$$K_{app} = K \exp\left(-\frac{\Delta z F \psi}{RT}\right) \tag{1}$$

where ψ is the surface potential (V), Δz is the net change of the surface charge caused by the formation of the surface complex, F is the Faraday's constant (96 485 C mol^{-1}), R is the universal gas constant (8.314 J $mol^{-1}{\cdot}K^{-1}$), and T is the absolute temperature (K).

The surface charge density is calculated by summing the molality of the charged surface components. The relationship between the rock's surface charge and the surface potential is given by the Grahame equation from the diffused layer model (Dzombak and Morel, 1990)

$$\sigma = \sqrt{8000 \varepsilon_r \varepsilon_0 RTI} \sinh\left(\frac{F\psi}{2RT}\right) \tag{2}$$

where I is the solution ionic strength ($mol{\cdot}dm^{-3}$), ε_r is the relative permittivity of the solution (78.5 for water at 25 °C), and ε_0 is the permittivity of free space (8.854×10^{-12} $C{\cdot}V^{-1}{\cdot}m^{-1}$).

The Debye-Hückel equation is used to estimate the zeta potential, ζ (V), from the surface potential calculated by the SCM.

$$\zeta = \psi e^{-\kappa d_s} \tag{3}$$

where κ is the inverse of the Debye length and d_s is the slip plane, estimated using the correlation proposed by Heberling et al. (2011).

$$d_s = \frac{0.13}{\sqrt{I}} \text{ (nm)} \tag{4}$$

The surface complexation reactions considered in this work are in Table 1. The equilibrium constants for reactions S1 to S6 are from Brady et al. (2012). This set of reactions has been widely used to replicate the experimental results of low-salinity waterflooding (Qiao et al., 2016; Sanaei et al. 2019) and to match zeta potential measurements of calcite and carbonate rocks (Tetteh et al., 2020).

The adsorption of glycine anion onto the calcite rock is described by reaction S7, where its K value was tuned based on zeta potential measurements with synthetic calcite (Lara Orozco et al., 2021). The aqueous reactions in Table 2 describe the speciation of glycine as a function of the solution pH. Their equilibrium constants at 95 °C are estimated using the extended van't Hoff equation for glycine proposed in Clarke et al. (2005).

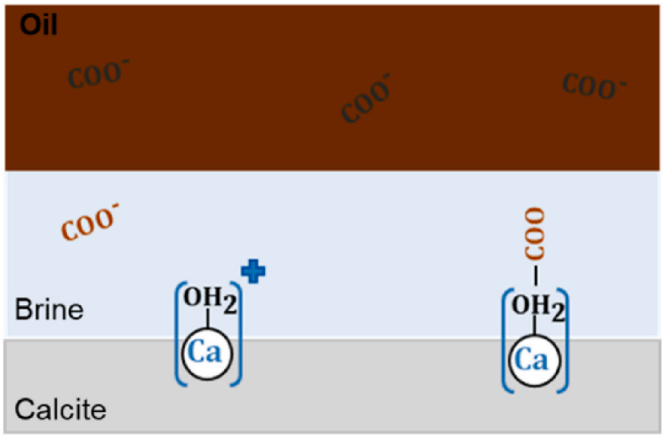

Fig. 2. Schematic of the adsorption of carboxylic acid, COO^-, onto the positively-charge surface component $> CaOH_2^+$. The concentration of COO^- in equilibrium with the rock surface is approximated by the total acid number (TAN) of the crude oil.

The described geochemical model was implemented in the open-source, geochemical solver PHREEQC v3.6.2 (Parkhurst, 1995) developed by the United States Geological Survey (USGS) using the PHREEQC database for the aqueous complexation reactions. The impact of calcite dissolution was neglected to focus on the impact of the adsorption of ions on the wetting state of the rock.

2.2. Wettability alteration model of carbonate rocks

Following Qiao et al. (2016), Sharma and Mohanty (2018), and Eftekhari et al. (2017), the wetting state of the rock is considered a function of the amount of carboxylic acid adsorbed onto the rock surface (Fig. 2). This is described in the SCM by reaction S8 in Table 1. The equilibrium constants are from Eftekhari et al. (2017) based on the analogous aqueous phase reaction.

The amount of carboxylic acid is determined by the crude oil total acid number, TAN (mg KOH/g-oil), (Erzuah et al., 2019):

$$COO = \frac{TAN}{1000 a_{oil} MW_{KOH}} \tag{5}$$

where COO is the concentration of carboxylic acids ($mol \cdot L^{-1}$) in equilibrium with the rock surface, a_{oil} is the specific surface area of oil ($m^2 \cdot g^{-1}$), and MW_{KOH} is the molecular weight of potassium hydroxide (56.1 g mol^{-1}). The specific surface area of the oil, a_{oil}, was taken to be equal to the rock's specific surface area.

The improved oil recovery obtained by wettability alteration is modeled by the change of the relative permeabilities curves as a linear function of the adsorbed concentration of carboxylic acids:

$$\omega = \frac{[> CaOH_2COO] - [> CaOH_2COO]_{ww}}{[> CaOH_2COO]_{ow} - [> CaOH_2COO]_{ww}} \tag{6}$$

where ω is used to interpolate between the oil-wet (ow) and water-wet (ww) relative permeability curves.

$$k_{r\alpha} = \omega k_{r\alpha}^{ow} + (1-\omega) k_{r\alpha}^{ww}, \alpha = o, w \tag{7}$$

Glycine and SO_4^{2-} anions act as wettability modifiers by adsorbing on calcite surface and decreasing the concentration of $> CaOH_2COO$. This is modeled by reactions S2, S7 and S8 in Table 1. A schematic of the desorption of COO by glycine and sulfate anions is in Fig. 3.

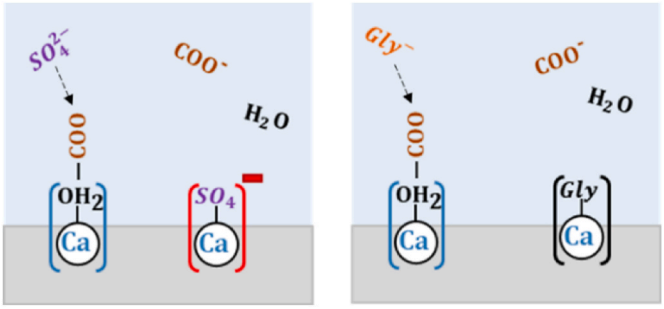

Fig. 3. Schematics describing the wettability alteration occurring by the removal of carboxylic acids by the adsorption of sulfate ion and glycine anion.

2.3. Analytical solution of injection of wettability modifiers

Here we present the derivation of the analytical model for the two-phase flow multicomponent reactive transport of ions in solution. The derivations follow the work of Pires et al. (2006), Khorsandi et al. (2017), Borazjani et al. (2019), Pope (1980), and Venkatraman et al. (2014).

2.3.1. Modeling wettability alteration by anion exchange reactions

The surface complexation reactions, S2, S3, S7, and S8, describe the desorption of carboxylic acids, COO^-, from the positively-charged surface components, $> CaOH_2^+$, by the adsorption of SO_4^{2-}, CO_3^{2-}, and Gly^-. Considering SO_4^{2-} and Gly^- as the main wettability modifiers, we propose the following anion exchange reactions:

$$2COOX + SO_4^{2-} \Longleftrightarrow SO_4X_2 + 2COO^- \tag{8}$$

$$COOX + Gly^- \Longleftrightarrow GlyX + COO^- \tag{9}$$

or as half-reactions:

$$X^+ + COO^- \Longleftrightarrow COOX \tag{10}$$

$$2X^+ + SO_4 \Longleftrightarrow COOX \tag{11}$$

$$X^+ + Gly^- \Longleftrightarrow GlyX \tag{12}$$

The K values of Equations (8) and (9) and the total surface sites of X^+ and k values can be obtained from calcite's surface complexation model using PHREEQC.

2.3.2. Governing equations for two-phase flow multicomponent reactive-transport

The 1D displacement of oil by an aqueous solution with n components considering incompressible fluids, homogeneous reservoir with negligible capillary pressure, diffusion, and dispersion, can be described by:

$$\frac{\partial s}{\partial t} + \frac{\partial f}{\partial x} = 0 \tag{13}$$

$$\frac{\partial (\mathbf{c}s + \mathbf{a})}{\partial t} + \frac{\partial \mathbf{c}f}{\partial x} = 0 \tag{14}$$

where s is the water saturation, f is the water fractional flow, $\mathbf{c}$ is the vector of equivalent ion concentrations in the aqueous phase, $\mathbf{a}$ is the vector of ion concentrations adsorbed on the rock surface.

Here x_D and t_D represent the dimensionless distance and time, respectively.

$$x_D = \frac{x}{L} \tag{15a}$$

$$t_D = \frac{ut}{\varphi L} \tag{15b}$$

where x is the spatial coordinate, t is time, L is the system length, φ is the porosity, and u is the total two-phase flux.

Equations (13) and (14) are subject to the following initial and boundary conditions:

$$t_D = 0 : \mathbf{c} = \mathbf{c}^I, s = s^I \tag{16a}$$

$$x_D = 0 : \mathbf{c} = \mathbf{c}^J, f = 1 \tag{16b}$$

where the fractional flow is defined as:

$$\mathrm{f} = \left(1 + \frac{\mathrm{k_{ro}}\,\mu_\mathrm{w}}{\mathrm{k_{rw}}\mu_\mathrm{o}}\right)^{-1} \tag{17}$$

The fractional flow depends not only on the water saturation, but also on the concentration of ions in the aqueous phase; i.e., $f = f(s, \mathbf{c})$. The latter dependence comes from the concentration of adsorbed carboxylic acids, $c_0 = \mathrm{COOX}$, that represents distinct wetting states of the rock surface through relative permeabilities.

2.3.3. Splitting two-phase system

The splitting procedure introduces the stream function to obtain exact solutions of two-phase waterflooding with ion exchange:

$$\varphi(x_D, t_D) = \int_{0,0}^{x_D, t_D} f dt_D - s dx_D \tag{18}$$

where it follows from Equation (18):

$$s = -\frac{\partial \varphi}{\partial x_D}, f = \frac{\partial \varphi}{\partial t_D} \tag{19}$$

$$d\varphi = f dt_D - s dx_D \tag{20}$$

Changing the coordinates from (x_D, t_D) to (x_D, φ), Equations (13) and (14) become

$$\frac{\partial\left(sf^{-1}\right)}{\partial \varphi} - \frac{\partial\left(f^{-1}\right)}{\partial x_D} = 0 \tag{21}$$

$$\frac{\partial \mathbf{a}}{\partial \varphi} + \frac{\partial \mathbf{c}}{\partial x_D} = 0 \tag{22}$$

The mapping to the new coordinates splits the system of equations into an auxiliary system for the single-phase reactive transport of ions (Equation (22)) and a scalar equation for two-phase flow (Equation (21)). The initial and boundary conditions for Equation (21) are transformed to

$$\varphi = -s^I x : s = s^I \tag{23a}$$

$$x_D = 0 : f = 1 \tag{23b}$$

For Equation 22

$$\varphi = -s^I x_D : \mathbf{c} = \mathbf{c}^I \tag{24a}$$

$$x_D = 0 : \mathbf{c} = \mathbf{c}^J \tag{24b}$$

The reactive transport of ions in Equation (22) is decoupled from Equation (21). The solution procedure consists of first solving the auxiliary system for the single-phase reactive transport of ions and then map the concentrations onto the fractional flow curves as explained in section 2.3.3.

2.3.4. Solution of single-phase flow with anion exchange reactions

Here we derive the analytical solution for single-phase flow with anion exchange reactions. The assumptions are

- The anion exchange capacity, Z, is a constant.
- The reactions are at local equilibrium.
- Dispersion is negligible.
- Ideal solutions, i.e., the activity of chemical components is equal to their molar concentrations.

Consider the transport of three adsorbing ions ($\mathrm{i} = 0, 1, 2$) and one non-adsorbing ion ($\mathrm{i} = 3$) in a single-phase system. In this derivation, component 0 is COO^-, a monovalent anion, component 1 is SO_4^{2-}, a divalent anion, component 2 is Gly^-, a monovalent anion, and component 3 is Na^+, a monovalent cation. The ion exchange reactions between anion 0 and anions 1 and 2 are:

$$k_{10} = \frac{a_1 c_0^2}{a_0^2 c_1} \tag{25}$$

$$k_{20} = \frac{a_2 c_0}{a_0 c_2} \tag{26}$$

where a_i and c_i are adsorbed and flowing concentrations of component i, respectively.

The two other equations are obtained from the electroneutrality condition and the volumetric anion exchange capacity of the rock, Z:

$$\mathrm{c}_0 + \mathrm{c}_1 + \mathrm{c}_2 = \mathrm{c}_3 \tag{27}$$

$$a_0 + a_1 + a_2 = \mathrm{Z} \tag{28}$$

The derivative $\frac{\partial \mathbf{a}}{\partial \varphi}$ in Equation (22) can be expressed in terms of $\mathbf{c}$ using the chain rule:

$$\mathbf{A}\frac{\partial \mathbf{c}}{\partial \varphi} + \frac{\partial \mathbf{c}}{\partial x_D} = \mathbf{0} \tag{29}$$

where

$$A = \begin{bmatrix} a_{11} & a_{12} & a_{13} \\ a_{21} & a_{22} & a_{23} \\ 0 & 0 & 0 \end{bmatrix}, a_{ij} = \frac{\partial a_i}{\partial c_j} \tag{30}$$

The system of PDEs in Equation (30) can be converted to a decoupled system of ODEs by introducing the similarity variable $\sigma = \frac{\varphi}{x_D}$:

$$(\mathbf{A} - \sigma \mathbf{I})\frac{d\mathbf{c}}{d\sigma} = \mathbf{0} \tag{31}$$

The system of ODEs in Equation (31) is decoupled by obtaining the eigenvalues and eigenvectors of **A.** The eigenvalues of Equation (31) are:

$$\sigma_1 = \frac{a_{11} + a_{22} - \sqrt{(a_{11} - a_{22})^2 + 4a_{12}a_{21}}}{2} \tag{32}$$

$$\sigma_2 = \frac{a_{11} + a_{22} + \sqrt{(a_{11} - a_{22})^2 + 4a_{12}a_{21}}}{2} \tag{33}$$

$$\sigma_3 = 0 \tag{34}$$

and the eigenvector for σ_1 and σ_2 are:

$$e_i = \begin{bmatrix} \frac{a_{11} - \sigma_i}{a_{12}} \\ 1 \\ 0 \end{bmatrix}, i = 1, 2 \tag{35}$$

The single-phase reactive transport problem is defined by the initial concentrations $\mathbf{c}^I$, the injection concentrations $\mathbf{c}^J$, the anion exchange capacity of the rock surface, Z, and the equilibrium constants for the anion exchange reactions, k_{01} and k_{02}. The solution consists of determining the two intermediate points, $\mathbf{c}^P$ and $\mathbf{c}^Q$, between the initial, $\mathbf{c}^I$, and injected, $\mathbf{c}^J$, concentrations separated by one cation wave, $\mathscr{W}_1$, and two anion waves, $\mathscr{W}_2$ and $\mathscr{W}_3$:

Table 3
Ionic composition of the brines studied by Lara Orozco et al. (2020).

Brine	Ion concentrations, ppm						I[a] mol/kg water	TDS[b] ppm
	Ca^{2+}	Mg^{2+}	Na^{+}	Cl^{-}	SO_4^{2-}	HCO_3^{-}		
FB	19 080	2561	70 991	150 165	588	186	6.37	243 571
SW	2880	536	22 928	40 500	1765	366	1.36	68 975
LSW	288	54	2293	4050	177	37	0.13	6898

[a] Ionic Strength.
[b] Total Dissolved Solids.

$$\mathbf{c}^J \overset{\mathscr{W}_3}{\rightarrow} \mathbf{c}^Q \overset{\mathscr{W}_2}{\rightarrow} \mathbf{c}^P \overset{\mathscr{W}_1}{\rightarrow} \mathbf{c}^I \tag{36}$$

The first intermediate point, $\mathbf{c}^P$, is obtained by considering that along with the eigenvector equation of $\sigma_3 = 0$; hence, the adsorbed concentrations, a_1 and a_2, are constant. The concentrations $\mathbf{c}^P$ are then obtained from the electroneutrality condition (Equation (28)) and the ion exchange reactions (Equations (25) and (26)):

$$\left[\frac{a_{1I}}{a_{0I}^2 k_{10}}\right] c_{0P}^2 + \left[\frac{a_{2I}}{a_{0I} k_{20}} + 1\right] c_{0P} - c_{3J} = 0 \tag{37}$$

The concentration of component 0 at the first intermediate point, c_{0P}, is obtained by solving the quadratic equation in Equation (37). The flowing concentrations, c_{1P} and c_{2P}, are obtained from the law of mass actions in Equations (25) and (26).

The following step is to determine $\mathbf{c}^Q$ which is connected to $\mathbf{c}^P$ and $\mathbf{c}^J$ by the anion waves $\mathscr{W}_2$ and $\mathscr{W}_3$. These waves can be shocks or rarefactions. In the case of rarefactions, the compositions are obtained by solving the ordinary differential equations obtained from the eigenvector of σ_2 and σ_3 in Equation (35) (Lake et al., 2014):

$$\frac{dc_1}{dc_2} = \frac{a_{12}}{\sigma_i - a_{11}}, i = 1, 2 \tag{38}$$

The concentrations from $\mathbf{c}^J$ to $\mathbf{c}^Q$, connected by $\mathscr{W}_3$, are obtained by integrating Equation (38).

The characteristic velocities of the concentration waves, λ, are obtained from the eigenvalues in Equations (32) and (33),

$$\lambda_i = \frac{1}{\sigma_i} \tag{39}$$

The type of wave is defined after comparing the characteristic velocities of $\mathbf{c}^P$, $\mathbf{c}^Q$, and $\mathbf{c}^J$. $\mathscr{W}_3$ is a rarefaction (spreading) wave if $(\lambda_3)_Q > (\lambda_3)_J$, else it is a shock. Similarly, $\mathscr{W}_2$ is a rarefaction wave if $(\lambda_2)_P > (\lambda_2)_Q$, else it is a shock. If the wave is shock, its velocity ($\widetilde{\lambda} = 1/\widetilde{\sigma}$) is calculated from the Rankine-Hugoniot jump condition:

$$\widetilde{\sigma} = \frac{(a_R + c_R) - (a_L + c_L)}{c_R - c_L} \tag{40}$$

where c_L and c_R correspond to the upstream and downstream compositions, respectively.

2.3.5. Mapping to fractional flow curves

Taking the derivative of Equation (20) with respect to x_D,

$$\frac{d\varphi}{dx_D} = f\frac{dt_D}{dx_D} - s \tag{41}$$

Let us define the characteristic speeds D and V in the coordinates (x_D, t_D) and (x_D, φ), respectively, as:

$$D = \frac{dx_D}{dt_D}, V = \frac{dx_D}{d\varphi} \tag{42}$$

Equation (41) then becomes

$$\frac{1}{V} = \frac{f}{D} - s \tag{43}$$

Finally, solving for D.

$$D = \frac{f}{s + \frac{1}{V}} \tag{44}$$

Equation (44) relates the characteristic velocities of the concentration waves in the coordinates (x_D, φ) and (x_D, t_D). The velocities of the concentration waves in the coordinates (x_D, t_D) are calculated using the characteristic velocities, λ_i, obtained from Equation (39) for rarefactions or the shock velocity, $\widetilde{\lambda}_i$, using Equation (40).

3. Results and discussion

This section first presents and discusses the results of the numerical solution of 1D reactive transport using calcite's SCM for the displacement of formation brine (FB) by seawater (SW), low salinity seawater (LSW), and seawater with 5 wt% glycine (SW-Gly5). Then, the k values of the anion exchange reactions for sulfate, glycine, and carboxylic acids are obtained from equilibrium calculations with varying concentrations in FB, SW, and LSW. Finally, we compare the analytical solutions for conventional waterflooding and the injection of seawater with 1 wt% and 5 wt% glycine.

3.1. Modeling wettability alteration by the adsorption of carboxylic acids

This section presents results from equilibrium geochemical calculations and two-phase flow simulations to investigate the impact of the adsorption of carboxylic acids on incremental oil recovery and how to reduce the SCM into a couple of anion exchange reactions.

3.1.1. Impact of K and COO on incremental oil recovery by wettability alteration

Several studies have reported that the wettability of carbonates is controlled by the adsorption of acidic components in the crude oil. This is described in the SCM by the surface complexation reaction S8 in Table 1. Expressing this reaction in terms of mass law action:

$$\mathrm{K} = \frac{[> \mathrm{CaOH_2COO}]}{[> \mathrm{CaOH_2^+}][\mathrm{COO^-}]} \mathrm{e}^{\left(-\frac{\Delta z F \Psi}{RT}\right)} \tag{45}$$

Applying the logarithm base 10 to both sides and reordering the terms:

$$\log \frac{[> \mathrm{CaOH_2COO}]}{[> \mathrm{CaOH_2^+}]} = \log \mathrm{K} + \log[\mathrm{COO^-}] - \frac{\log\left(-\frac{\Delta z F \Psi}{RT}\right)}{\ln(10)} \tag{46}$$

The left side of Equation (46) is equivalent to the fraction of the rock surface that is covered by carboxylic acids, because $> \mathrm{CaOH_2^+}$ is the dominant component at the typical pH values encountered in field brines.

The equilibrium constant in Equation 46, K, represents the affinity of carboxylic acids for the carbonate surface. Its value is estimated by matching the oil recovery obtained in spontaneous imbibition and coreflood experiments. This is because COO is a pseudo component representing an unknown mixture of acidic compounds present in the crude oil. The main components known to influence carbonate's wettability

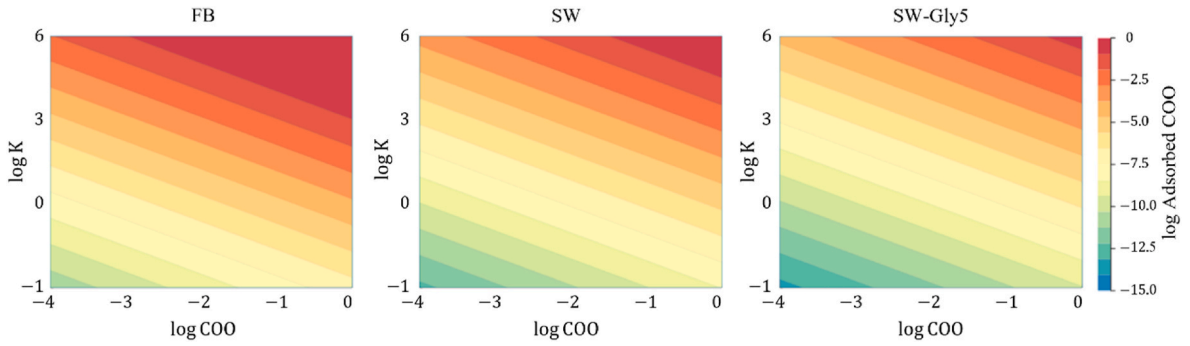

Fig. 4. Equilibrium concentration of adsorbed carboxylic acids as a function of K of reaction S8 and aqueous concentration of carboxylic acids for a) Formation Brine (FB), b) Seawater (SW), and c) Seawater with 5 wt% glycine (SW-Gly5).

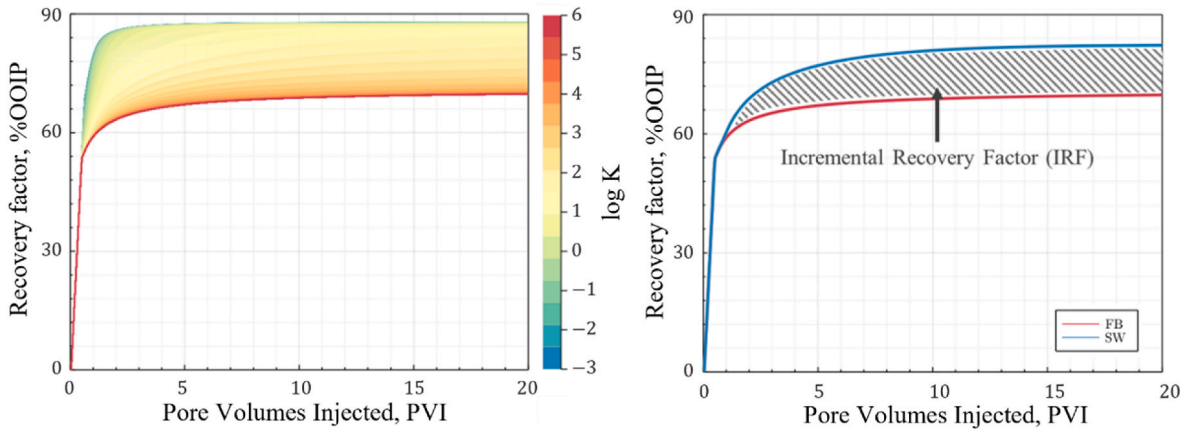

Fig. 5. Recovery factor by the injection of seawater (SW) and formation brine (FB). The incremental oil recovery factor is calculated by integrating between both recovery factor curves from 0 to 20 PVI.

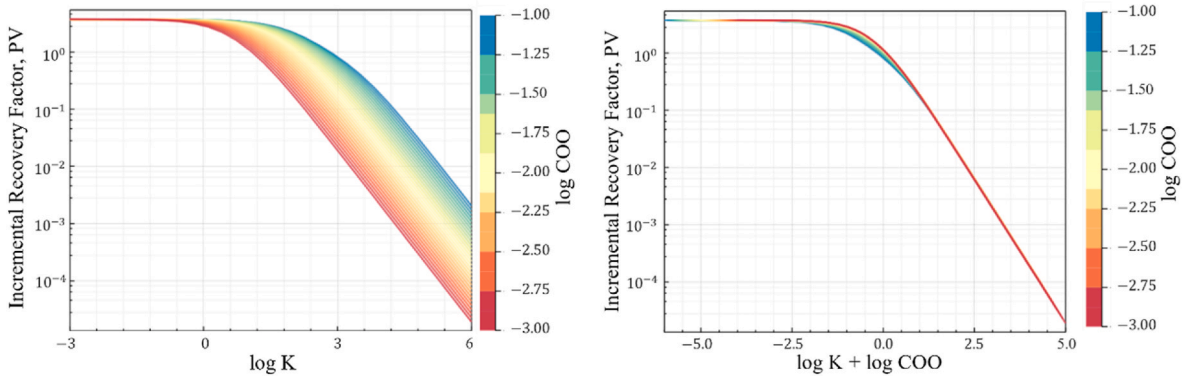

Fig. 6. Incremental recovery factor by injection of seawater (SW) as a function of a) log K and b) log K + log COO. The incremental recovery curves collapsed when plotted against log K + log COO.

are long chain fatty acids, long chain naphthenic acids, and asphaltenes (Al-Busaidi et al., 2019; Tessarolo et al., 2021). The equilibrium constant, K, represents the overall chemical interaction of these acidic compounds with the carbonate surface. Hence, K may take values within a range of several orders of magnitude.

The concentration of carboxylic acids in equilibrium with the rock surface is represented by COO. As discussed in section 2.2, COO in mol/L is calculated from the crude oil TAN in mg KOH/g oil. It has been observed that the carbonate surface becomes more oil wet as the TAN increases (Zhang and Austad, 2005; Fathi et al. 2010). However, the TAN only quantifies the bulk concentration of acidic compounds without accounting for the structure of the acidic compounds, e.g., chain length and aromaticity (Bonto et al., 2019). Therefore, TAN might not be a good indicator of the extent and type of acidic compounds that partition into the aqueous phase to adsorb on the rock surface.

Given the uncertainties in the values of K and COO, their impact on the adsorption of carboxylic acids was investigated by a sensitivity analysis using the SCM. The speciation of the carbonate surface was calculated in equilibrium with FB, SW, and SW-Gly5. The ionic compositions of these brines are in Table 3. The range of K values investigated are based on the values reported in the literature (Qiao et al., 2016; Chandrasekhar et al., 2018; Eftekhari et al., 2017). The range of

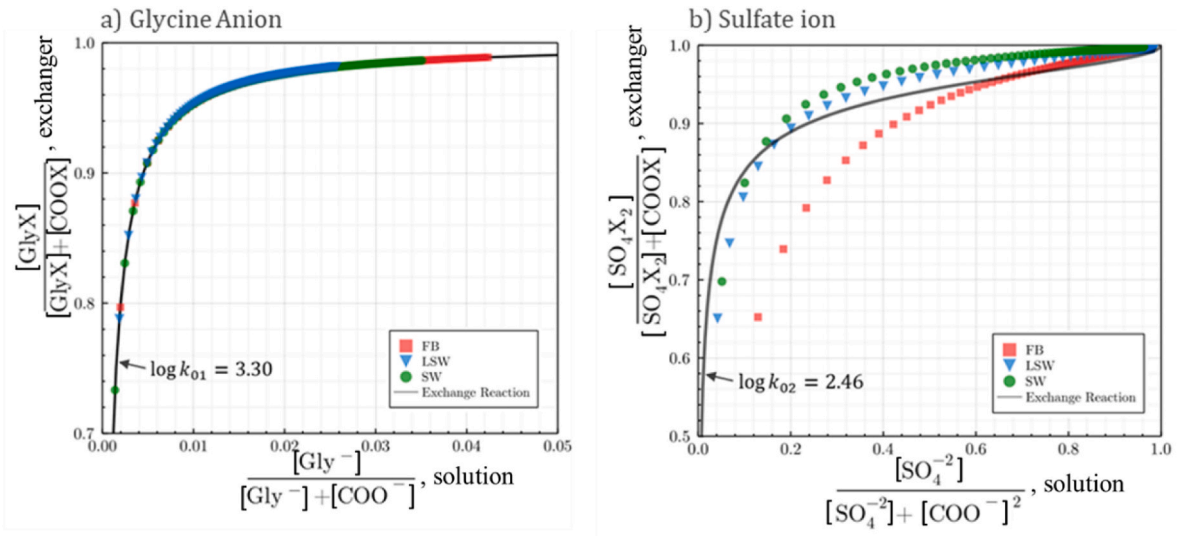

Fig. 7. Adsorption isotherm of COO^-, Gly^-, and SO_4^{2-} as a function of the aqueous concentration a) glycine anion and b) sulfate ion with their corresponding k values for the anion exchange reaction in Equation (8) and Equation (9).

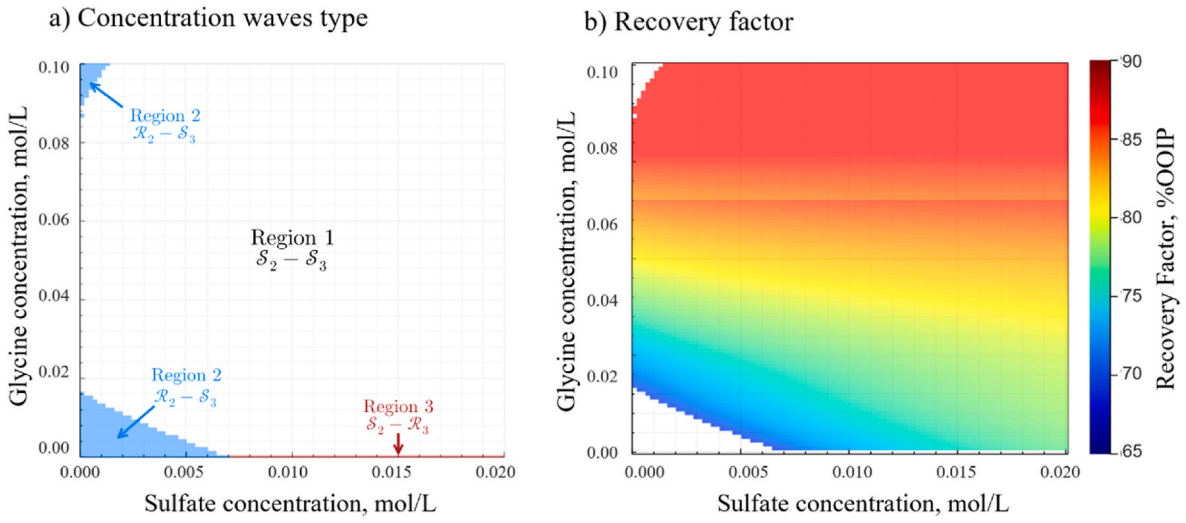

Fig. 8. a) Type of concentration waves, $\mathscr{W}_2 - \mathscr{W}_3$, for the injection of seawater with 5 wt% glycine. $\mathscr{S}_i$ and $\mathscr{R}_i$ indicates wheter $\mathscr{W}_i$ is a shock or rarefaction, respectively. b) Recovery factor after 10 IPV as a function of glycine and sulfate concentration obtained from the analytical solution of two-phase flow problem with anion exchange reactions.

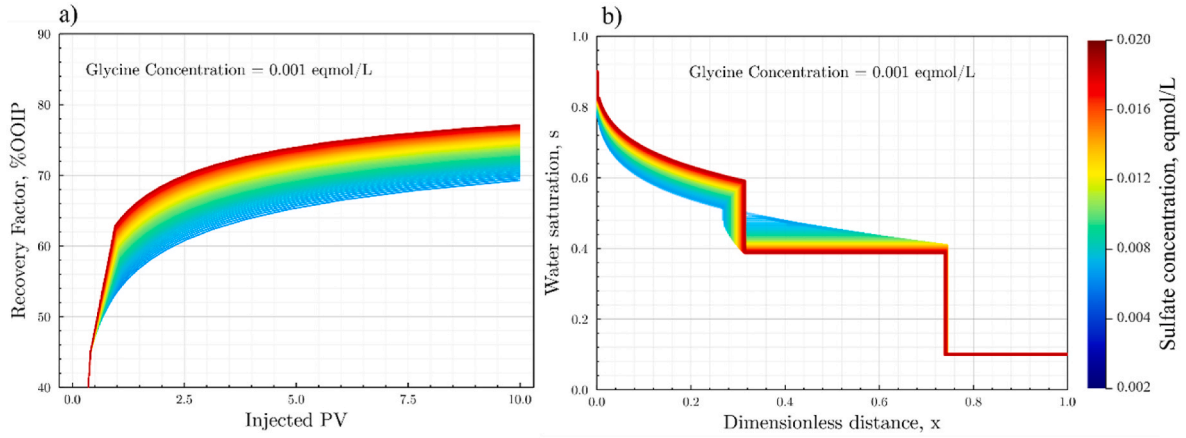

Fig. 9. a) Recovery factor curves and b) water saturation profile at 0.30 PVI as a function of sulfate concentration for a fixed glycine concentration of 0.001 eqmol/L.

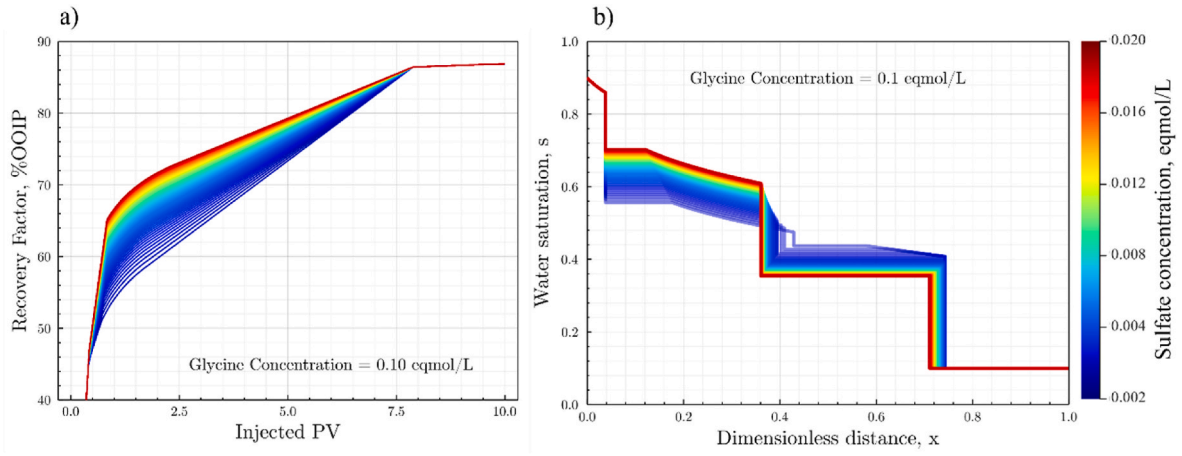

Fig. 10. a) Recovery factor curves and b) water saturation profile at 0.30 PVI as a function of sulfate concentration for a fixed glycine concentration of 0.1 eqmol/L.

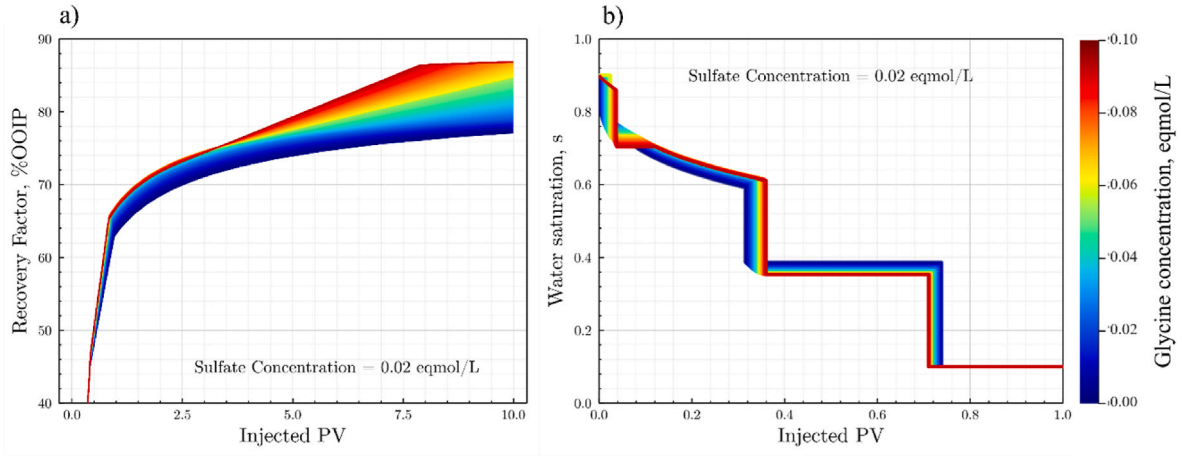

Fig. 11. a) Recovery factor curves and b) water saturation profile at 0.30 PVI as a function of glycine concentration for a fixed sulfate concentration of 0.02 eqmol/L.

Table 6
Relative permeability parameters for water-wet, oil-wet, and intermediate states for the injection of SW-Gly5. The Corey-Brooks parameters of the water-wet and oil-wet cases are from Sharma and Mohanty (2018). The wettability index, ω, is obtained from the adsorbed concentration of carboxylic acids using Equation (6). The parameters for the mixed-wet state are found from using Equation (7).

Parameter	Water-Wet $\omega = 0.008$	Oil-Wet $\omega = 1$	Mixed-Wet $\omega = 0.447$
s_{wr}	0.11	0.11	0.11
s_{or}	0.10	0.16	0.12
k^0_{rw}	0.2	0.4	0.29
k^0_{ro}	0.79	0.5	0.66
n_w	3	2	2.55
n_o	2	3	2.44

COO values corresponds to TAN values ranging from 0.1 to 5 mg KOH/g oil (Bonto et al., 2019).

Fig. 4 shows that the concentration of adsorbed carboxylic acids is linearly dependent on log K and log COO for all the three solutions: FB, SW, and SW-Gly5. This is explained by Equation (46). The linear dependency, however, is not necessarily obvious because the surface and aqueous complexation reactions require the solution of a set of nonlinear algebraic equations. Hence, a single parameter consisting of log K+ log COO should be used to characterize the wetting state of carbonate rocks.

The difference in the amount of adsorbed carboxylic acids between the solutions occurs because of the higher concentration of sulfate in SW and the addition of glycine in SW-Gly5. These chemicals adsorb onto the calcite surface according to reactions S2 and S7 in Table 1, displacing carboxylic acids. The reduction of the surface potential also influences the removal of carboxylic acids. The impact of the surface potential is accounted for by the last term on the right side of Equation (46). The lower concentration of calcium and magnesium in SW, in comparison to FB, results in their desorption described by reactions S5 and S6 in Table 1. Consequently, the surface potential decreases. This is the main mechanism of low salinity waterflooding.

We further investigated the impact of K and COO on the incremental recovery factor (IRF). obtained by wettability alteration. A numerical model of 1D displacement was coupled with the SCM to simulate wettability alteration by the injection of SW. Fig. 5a shows the recovery factor curves calculated for different log K and log COO values. The curves are colored by log K. The IRF was calculated for each curve by calculating their area up to 20 pore volumes of injection (PVI) with respect to the oil-wet case, as shown in Fig. 5b.

The results of the sensitivity analysis are in Fig. 6a. Here the IRF is plotted as a function of log K and colored by log COO. In this case, there is a critical log K value of approximately zero. Below this value, strong water-wetting conditions are obtained regardless of log COO. For log K values greater than zero, larger log COO values result in smaller IRF. The most relevant result comes from plotting the IRF as a function of log K + log COO. Fig. 6b shows that all of the IRF curves collapse into a single curve. It means that similar values of log K + log COO will result in

similar wettability alteration and displacement efficiency by the injection of SW.

There are two important consequences of the linear trends observed for the adsorption of carboxylic acids and the incremental oil recovery as a function of log K and log COO. First, it means the wetting state of the carbonates represented by the amount of adsorbed carboxylic acids can be characterized by a single parameter obtained from adding up log K and log COO. Second, since the log K and log COO terms in Equation (46) are more important than the change of surface potential, we can focus on modeling the impact of wettability modifiers in terms of their adsorption and displacing of carboxylic acids. This significantly reduces the SCM into a set of anion exchange reactions.

3.1.2. Modeling wettability alteration by anion exchange reactions

Previous sections showed that the rock's wetting-state and incremental oil recovery by wettability alteration can be largely characterized by $\log K + \log COO$. Likewise, wettability alteration can be further simplified by reducing the SCM into a set of anion exchange reactions between carboxylic acids and wettability modifiers. The equilibrium constants for these anion exchange reactions are obtained by running equilibrium calculations in PHREEQC with varying concentrations of glycine and sulfate.

The adsorption isotherms between glycine and carboxylic acids are in Fig. 7a. The adsorbed glycine concentration is expressed as a fraction of exchange sites occupied by glycine

$$\theta_{Gly} = \frac{GlyX}{GlyX + COOX} \tag{47}$$

θ_{Gly} is calculated with glycine concentrations varying from 0 to 0.6 mol/L (5 wt%) in FB, SW, and LSW. Fig. 7 shows a comparison of θ_{Gly} calculated with the SCM and the exchange reaction in Equation (9). A value of 3.30 for $\log k_{01}$ was used to match the results from the SCM.

Fig. 7b shows the adsorption isotherm between sulfate and carboxylic acid. The fraction of exchange sits occupied by sulfate is defined as

$$\theta_S = \frac{SO_4X_2}{SO_4X_2 + COOX} \tag{48}$$

θ_S was calculated in solutions prepared by adding up to 0.03 mols of Na_2SO_4 to FB, SW, and LSW. The θ_S values calculated with the exchange reaction in Equation (8) using $\log k_{02} = 2.46$ are in good agreement with the results from the SCM. The largest discrepancies occurred with FB. This is explained by the decrease in sulfate's activity in brines with high ionic strengths.

3.2. Impact of glycine and sulfate concentrations on recovery factor

The anion exchange constants in the previous section were obtained by matching the equilibrium calculations of the surface complexation model at varying concentrations of glycine and sulfate. These constants are used in this section to investigate the impact of glycine and sulfate on enhanced oil recovery using the analytical solutions described in section 2.3. A detailed solution for the injection of seawater with 5 wt% glycine is in Appendices A and B.

We first evaluated the influence of glycine and sulfate concentrations on whether the wettability waves are shocks or rarefactions. Fig. 8a shows the different combinations of wave types for $\mathscr{W}_2$ and $\mathscr{W}_3$ as a function of glycine and sulfate aqueous concentration at the injection. Glycine wave, $\mathscr{W}_3$, is always a shock since there is no glycine initially in the system. Only a rarefaction occurs at glycine concentrations close to zero. $\mathscr{W}_2$ is a rarefaction at low sulfate concentrations. This is dependent on glycine's concentration. Increasing the glycine concentration promotes the formation of shocks for $\mathscr{W}_2$ at lower sulfate concentrations. This indicates a synergy between glycine and sulfate, where the addition of glycine improves the displacement efficiency by sulfate's wettability wave.

Fig. 8b shows contours of the recovery factor at 10 PVI as a function of glycine and sulfate concentrations at the injection. Recovery factor was only calculated at Region 1 where both wettability waves are shocks. This is because the two-phase solution with rarefied concentration waves requires the use of numerical methods, e.g., front-tracking algorithm (Khorsandi et al., 2017). The glycine concentration is shown to greatly impact the recovery factor because of its higher affinity for the rock surface that results in more water-state condition. The presence of sulfate increases the efficiency of glycine's injection.

Additional plots of recovery factor and saturation profiles are presented to understand the impact of glycine and sulfate on the displacement efficiency. Fig. 9a shows the recovery curve as a function of sulfate concentration with negligible glycine concentration. The increase in the sulfate concentration at the injection results in a more water-wet condition. The displacement efficiency is improved by the formation of a wettability shock caused by the desorption of carboxylic acids by sulfate anion, as shown in Fig. 9b.

We investigated the synergy between glycine and sulfate by varying their concentrations with respect to the base case: the injection of seawater with 5 wt% glycine. Fig. 10 shows the recovery factor curves and saturation profiles as a function of sulfate concentration with a glycine concentration of 0.1 eqmol/L that corresponds to a 5 wt% load. Increasing sulfate concentration does not change the velocity of glycine's wettability wave. Instead, the increasing recovery factor occurs by the formation of a faster wettability wave by sulfate. Fig. 11 shows recovery factor curves and saturation profiles at varying concentration of glycine at a fixed sulfate concentration of 0.02 eqmol/L. This corresponds to the sulfate concentration in seawater. As observed in the saturation profiles, increasing glycine concentration increases the velocity of both sulfate's and glycine's wettability shocks, that results in a faster oil recovery. Figs. 10 and 11 indicate a synergistic effect of glycine and sulfate on the displacement efficiency and the wettability shock velocities. Likewise, we can observe higher oil recovery by combining glycine and sulfate. For instance, at 5 PVI, 74% OOIP is recovered at high sulfate and low glycine concentrations (Figs. 9), 73% OOIP at high glycine and low sulfate concentrations (Fig. 10), while 80% OOIP at both high glycine and high sulfate concentrations. Hence, higher oil volume is recovered when combining glycine and sulfate.

4. Conclusions

This study investigated the impact of reactive transport of the wettability modifiers SO_4^{2-} and glycine on ultimate oil recovery in waterflooded carbonate reservoirs. The role of brine composition in wettability alteration was investigated by equilibrium geochemical calculations and the analytical solution of the two-phase reactive transport problem. Wettability alteration was modeled through anion exchange reactions between the adsorbed carboxylic acids and the injected wettability modifiers.

Based on results from the surface complexation model, we proposed anion exchange reactions between wettability modifiers, such as glycine anion Gly^- and sulfate ion SO_4^{2-}, and carboxylic acids COO^-. The desorption of COO^- represented the wettability alteration of the rock surface. The K values of the anion exchange reactions were obtained by running equilibrium calculation in PHREEQC with varying concentrations of sulfate and glycine. Finally, we presented analytical solutions for the coupled two-phase reactive transport model for enhanced waterflooding by wettability modifiers, glycine, and sulfate. The main conclusions of this research are as follows:

- The rock's wetting state and the incremental oil recovery are linearly correlated with log K corresponding to the adsorption of carboxylic acids and log COO calculated from the total acid number in the crude oil. Similar values of log COO + log K have the same initial and final

wetting states that result in equivalent waterflooding efficiencies. Therefore, waterflooding enhanced by wettability alteration can be characterized by a single parameter, $\log \mathrm{COO} + \log \mathrm{K}$.

- The main chemical reactions describing wettability alteration are the surface complexation reactions for the adsorption of glycine, sulfate, and carboxylic acids. The degree of desorption of carboxylic acids from the rock surface by injection of wettability modifiers, like sulfate and glycine anions, can be approximated by a reduced set of anion exchange reactions. The resulting physical model for the injection of wettability modifiers was sufficient for the analytical solutions without using a complete surface complexation model.
- Waterflooding with seawater enhanced by glycine increases oil recovery over waterflooding by the formation of one to two wettability-alteration shocks depending on the glycine concentration and the brine pH as they affect the activity of glycine anion.
- Although glycine desorbs both sulfate and carboxylic acids from a carbonate surface, a synergy was found between glycine and sulfate, where the presence of glycine promotes the formation of a wettability-alteration shock by sulfate that improves the displacement efficiency.

Declaration of competing interest

The authors declare that they have no known competing financial interests or personal relationships that could have appeared to influence the work reported in this paper.

Data availability

Data will be made available on request.

Acknowledgments

We acknowledge sponsors of the Energi Simulation Industrial Affiliate Program (IAP) on Carbon Utilization and Storage, and the IAP on Chemical EOR at the Center for Subsurface Energy and the Environment at the University of Texas at Austin. Ryosuke Okuno holds the Pioneer Corporation Faculty Fellowship in Petroleum Engineering at the University of Texas at Austin. Larry W. Lake holds the Shahid and Sharon Endowed Chair at the University of Texas at Austin.

Nomenclature

a_i	Concentration of adsorbed ion i, (eqmol·L^{-1})
$\mathrm{a_{oil}}$	Oil specific surface area (m^2·g^{-1})
c_i	Concentration of ion i in the aqueous phase, (eqmol·L^{-1})
$\mathrm{d_s}$	Slip plane (nm)
D	Characteristic speed in coordinates (x_D, t_D)
e	Elementary charge (1.602×10^{-19} C)
f	Water fractional flow
F	Faraday's constant (96 485 C mol^{-1})
I	Solution ionic strength (mol·dm^{-3})
$k_{r\alpha}$	Relative permeability of phase α
k_{ij}	Exchange constant between components i and j
κ	Inverse of the Debye length (nm^{-1})
$\mathrm{K_{app}}$	Apparent equilibrium constant
K	Intrinsic equilibrium constant
L	System length, m
$\mathrm{MW_{KOH}}$	Molecular weight of potassium hydroxide (56.1 g mol^{-1})
$\mathrm{N_A}$	Avogadro's number (6.022×10^{23} mol^{-1})
R	Universal gas constant (8.314 J mol^{-1}·K^{-1})
s	Water saturation
t	Time, s
t_D	Dimensionless time
T	Absolute temperature (K)
TAN	Total acid number (mg of KOH/g of oil)
u	Total flux, m·s^{-1}
V	Characteristic speed in coordinates (x_D, φ)
x	Distance, m
x_D	Dimensionless distance
Z	Volumetric anion exchange capacity, mol·L^{-1}
ε_0	Permittivity of free space (8.854×10^{-12} C·V^{-1}·m^{-1})
ε_r	Relative permittivity of the solution (78.5 for water at 25 °C)
Δz	Net change of surface charge
λ_i	Characteristic velocity of wave i
$\widetilde{\lambda}$	Shock velocity
σ	Surface charge density (C·m^{-2})
σ_i	Eigenvalue i
$\widetilde{\sigma}$	Shock retardation
ϕ	Porosity
φ	Flow potential
ψ	Surface potential (V)
ζ	Zeta potential (V)

Table A.1
Flowing concentration solutions and their corresponding retardation values obtained by the single-phase reactive transport problem of the injection of seawater with glycine 5 wt%.

Point	Flowing Concentrations ($\times 10^{-3}$ eq mmol/L)				σ_1	σ_2	$\tilde{\sigma}$	Wave Type
	c_0 *COO*	c_1 *S*	c_2 *Gly*	c_3 *Na*				
I	9	14	1×10^{-6}	23	–	–	0.0	Indifferent
P	26.53	121.68	2.94×10^{-6}	148.2	0.15	–	0.14	Shock
Q	12.5	3.1	3.1×10^{-6}	148.2	266.5	0.14	6.99	Shock
J	9	39.22	100	148.2	–	0.006	–	–

Appendix A. Single-Phase Reactive Transport of SW-Gly5

This Appendix presents examples of the solution of the single-phase reactive transport problem for the injection of seawater with 5 wt% glycine. The problem is defined in terms of the initial and injected concentrations, $\mathbf{c}^I$ and $\mathbf{c}^J$, and the exchange constants, k_{10} and k_{20}. The initial and injected concentrations are in Table A1. The anion exchange constants are in Fig. 7. The ionic concentration of sulfate in the initial and injected brines are similar to its concentration in FB and SW (Table 3), respectively. The concentrations of sodium cation were calculated using the electroneutrality condition.

First, the adsorbed concentration of component 0 at *I* are calculated by substituting Equations (25) and (26) into Equation (28).

$$\left[\frac{k_{10}c_{1I}}{c_{0I}^2}\right]a_{0I}^2 + \left[1+\frac{k_{20}c_{2I}}{c_{0I}}\right]a_{0I} - Z = 0 \tag{A.1}$$

From the solution of the quadratic equation:

$$a_{0I} = \frac{-1-\frac{k_{20}c_{2I}}{c_{0I}} + \sqrt{\left(1+\frac{k_{20}c_{2I}}{c_{0I}}\right)^2 + \frac{4Zk_{10}c_{1I}}{c_{0I}^2}}}{2\frac{k_{10}c_{1I}}{c_{0I}^2}} = 3.737 \times 10^{-3} \tag{A.2}$$

After solving for a_{0I}, the adsorbed concentrations of components 1 and 2 at *P* are obtained from Equations (25) and (26):

$$a_{1I} = \frac{k_{10}a_{0I}^2 c_{1I}}{c_{0I}^2} = 0.696 \; eqmol \Big/ L \tag{A.3}$$

$$a_{2I} = \frac{k_{20}a_0 c_{2I}}{c_{0I}} = 8.285 \times 10^{-3} \; eqmol \Big/ L \tag{A.4}$$

The concentrations at the first intermediate point, *P*, are also calculated from solving algebraic equations arising from Equations (25)–(28). Given that the eigenvalue for the cation wave is zero, $\sigma_3 = 0$, Equation (31) yields

$$\frac{d\hat{c}_1}{d\sigma} = 0 \text{ and } \frac{d\hat{c}_2}{d\sigma} = 0 \tag{A.5}$$

which indicates that the adsorbed concentrations of components 1 and 2 do not change along the cation wave, $\mathscr{W}_1$. Therefore, all the adsorbed concentrations at *P* are equal to the adsorbed concentrations at *I*:

$$\hat{\mathbf{c}}_P = \hat{\mathbf{c}}_I \tag{A.6}$$

Given that component 3 does not adsorb, $c_{3P} = c_{3J}$. The concentration of component 0 at *P* is obtained from solving the quadratic equation in Equation (37):

$$c_{0P} = \frac{-1-\frac{a_{2I}}{a_{0I}k_{20}} + \sqrt{\left(\frac{a_{2I}}{a_{0I}k_{20}}+1\right)^2 + 4c_{3J}\frac{a_{1I}}{a_{0I}^2 k_{10}}}}{2\frac{a_{1I}}{a_{0I}^2 k_{10}}} = 0.0265 \; eqmol \Big/ L \tag{A.7}$$

The flowing concentrations of components 1 and 2 at P are calculated from Equations (25) and (26):

$$c_{1P} = \frac{a_{1P}c_{0P}^2}{a_{0P}^2 k_{10}} = 0.121 \; eqmol \Big/ L \tag{A.8}$$

$$c_{2P} = \frac{a_{2P}c_{0P}}{a_{0P}k_{20}} = 2.948 \times 10^{-9} \; eqmol \Big/ L \tag{A.9}$$

The second intermediate point *Q* is found at the intersection of $\mathscr{W}_3$ and $\mathscr{W}_2$. The solution should satisfy the ODE in Equation (38) for both eigenvectors σ_1 and σ_2, Equations (32) and (33), respectively. For this, we numerically solve Equation (38) with σ_1 with c_2 ranging from c_{2P} to c_{2J}. Then, solve Equation (38) with σ_2 with c_2 ranging from c_{2J} to c_{2P}. This is shown in Fig. 8. The point where the two solutions meet is the concentration for the second intermediate point *Q*.

The concentrations from the solution of the single-phase reactive transport problem are in Table A1. The eigenvectors corresponding to each point are calculated using Equations (32) and (33). These are used to determine whether a wave is a shock or rarefaction:

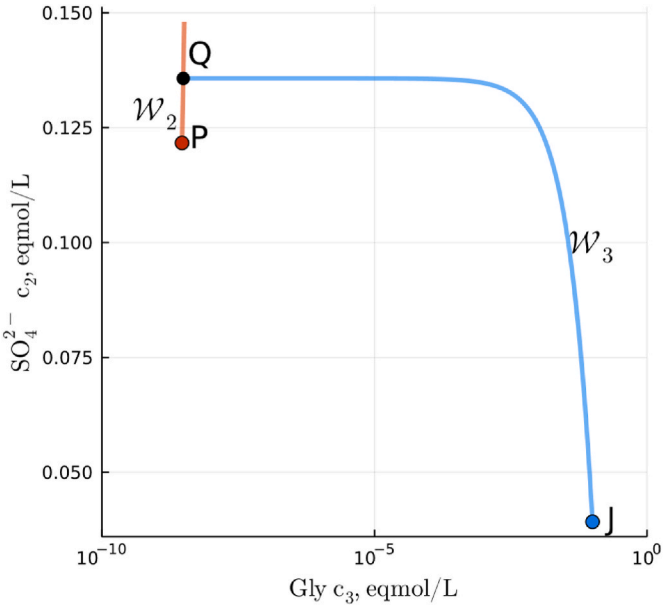

Fig. A.1. Solutions of the ODEs in Equation (34) to obtain the concentrations at point Q for SW injection with 5 wt% glycine.

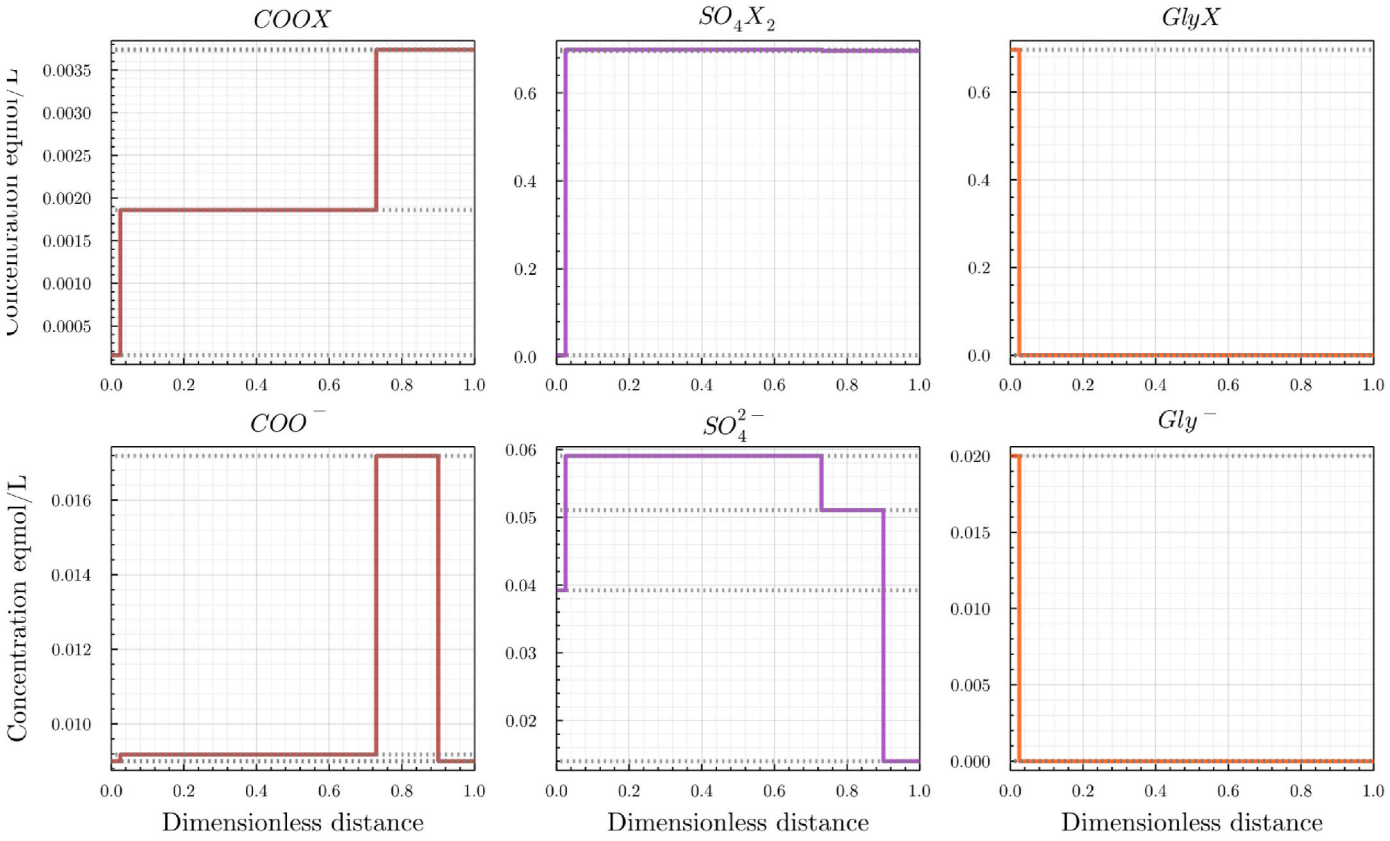

Fig. A.2. Flowing and adsorbed concentrations obtained from the solution of the single-phase reactive transport of seawater with 5 wt% glycine at 0.3 PVI.

$$\text{if } \sigma_{1Q} \geq \sigma_{2J} \therefore \mathscr{W}_3 \text{ is a shock} \tag{A.10}$$

$$\text{if } \sigma_{1P} \geq \sigma_{1Q} \therefore \mathscr{W}_2 \text{ is a shock} \tag{A.11}$$

A shock is formed if σ_1 at Q is greater or equal to σ_2 at J, because the wave velocity at J is greater than the wave velocity at Q. Similarly, a shock is formed when σ_1 at P is greater than σ_1 at Q because the wave at Q is faster than the wave at P. The shock retardations are then calculated using the Rankine-Hugoniot jump conditions given in Equation (40). The resulting shock retardations are in Table A1.

The concentration profiles of the flowing and adsorbed components at 0.30 pore volumes injected (PVI) are in Figure A2. The first wettability wave corresponds to the desorption of carboxylic acids caused by the higher concentration of SO_4^{2-} in SW compared to FB. At this same position, there is also

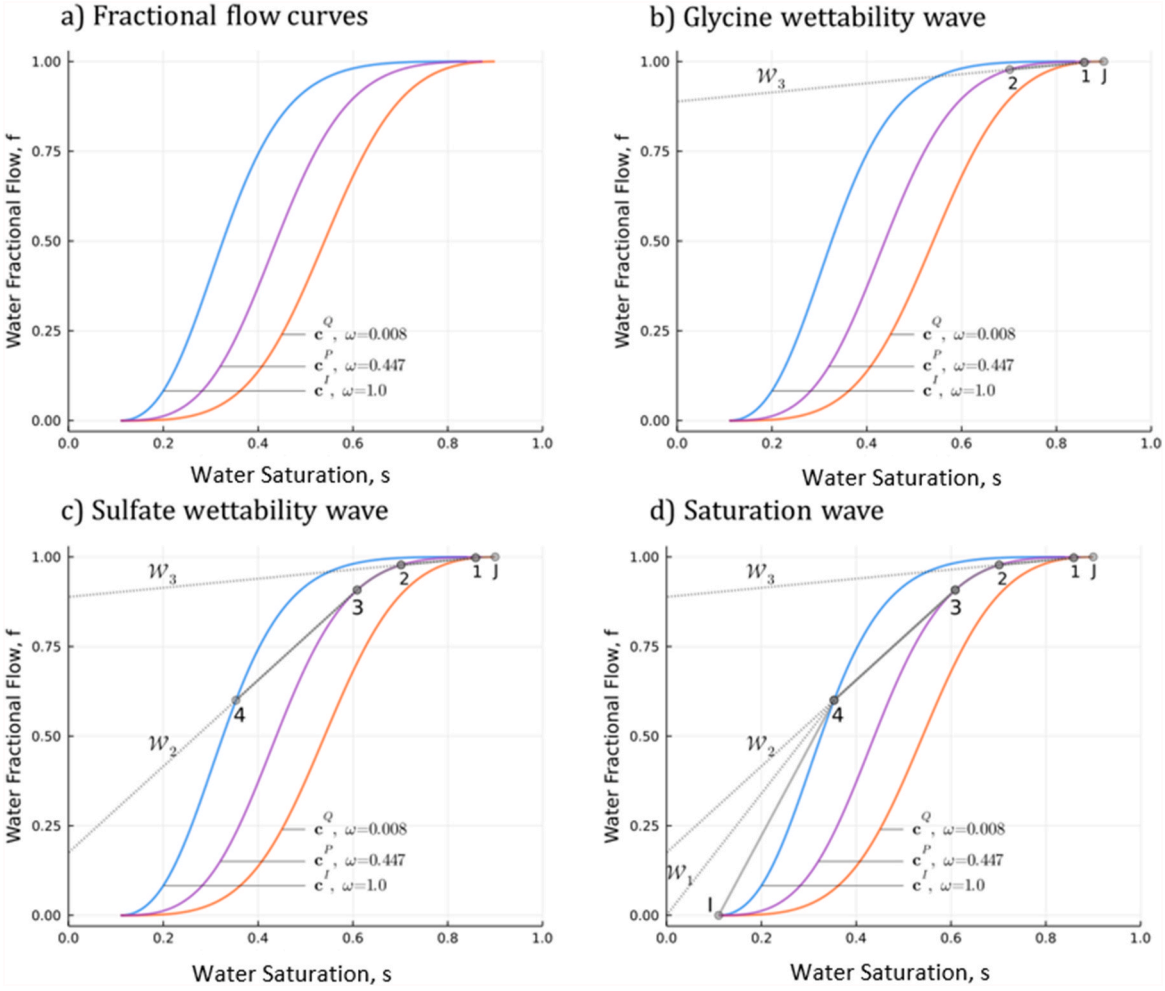

Fig. B.1. Mapping of fractional flow onto the concentration solutions $\mathbf{c}^J$, $\mathbf{c}^Q$, and $\mathbf{c}^P$ for conventional waterflooding and injection of SW-Gly1. The fractional curves are calculated using the Corey-Brooks parameters in Table 6.

a spike in the flowing concentration of COO^-. An increase of TAN in the effluent crude oil after the injection of anionic surfactants for wettability alteration has been previously reported in the literature (Mohammadi et al., 2019). There is a second wettability wave caused by the injection of glycine that greatly desorbs carboxylic acids related to a more water wetting state. Adsorbed sulfate is also removed by glycine to a lesser extent.

Appendix B. Two-Phase Flow Solution of SW-Gly5

The single-phase reactive transport of seawater with glycine 5 wt% results in the formation of two shocks corresponding to the increase of glycine and sulfate concentrations at the injection. These two shocks separate three distinct wetting states given by the reduction of the adsorbed carboxylic acids, *COOX*, as shown in Figure A2. The wettability index in Equation (6) is calculated from the concentration of *COOX* at each point in Table A1.

The fractional flow curves corresponding to each wetting state are in Figure B1a. The oil and water viscosities are 5 cP and 1 cP, respectively. The endpoint mobility ratios for the oil- and water-wet states are 4.94 and 1.25, respectively. For constant fluid viscosities, making the rock more water-wet is qualitatively equivalent to decreasing the endpoint mobility ratio (Lake et al., 2014).

The retardations of each wave are in Table A1. These are mapped onto the fractional flow curves to obtain the two-phase flow solution. The wave velocities in (x, φ) coordinates, V, are related to the velocities in (x, t) coordinates, D, according to Equation (44). Since, the wave retardation is the inverse of the specific wave velocity, $\frac{1}{V} = \sigma$, following Equation (44), the solution corresponds to a line connecting the points $(-\sigma, 0)$ and (s, f).

Figure B1b shows the solution for glycine's wettability wave, $\mathscr{W}_3$, where $\sigma = 6.99$. The solution consists of finding the line starting at $(-6.99, 0)$ that is tangent to the most water-wet fractional flow curve ($\omega = 0.008$). The slope of this line is 0.12. This is the specific velocity of glycine's wettability shock. The resulting line crosses the mixed-wet fractional flow curve ($\omega = 0.447$) at point 2. The solution consists of a rarefaction from J to 1 and a shock from 1 to 2.

A similar procedure is followed to obtain the solution for the sulfate's wettability wave, we just consider point 2 to be point J in the previous solution. Figure B1c shows the solution for $\mathscr{W}_3$ with $\sigma = 0.14$. The line starts at $(-0.14, 0)$ and its tangent to the fractional flow corresponding to the mixed-wet conditions with $\omega = 0.447$. The line crosses the oil-wet fractional flow curve ($\omega = 1.0$) at point 4. The specific velocity of the sulfate's wettability shock is 1.20. The solution then consists of a rarefaction from 2 to 3 and a shock from 3 to 4.

The solution of conventional waterflooding is obtained by considering point 4 as the injection point, J. This corresponds to the well-known Buckley Leverett solution in the fractional flow theory presented in Lake et al. (2014). In this case, the solution consists of a saturation shock from I to 4. The specific velocity of the cation wave, $\mathscr{W}_1$, which is indifferent, is calculated from the slope of the line connecting the points $(0, 0)$ and $(s_4, f(s_4))$. Here s_4

is the water saturation at point 4 and f is the oil-wet fractional flow ($\omega = 1.0$). Finally, Figure B2 shows the water saturation profile corresponding to the injection of seawater with 5 wt% glycine at 0.35 pore volumes injected (PVI).

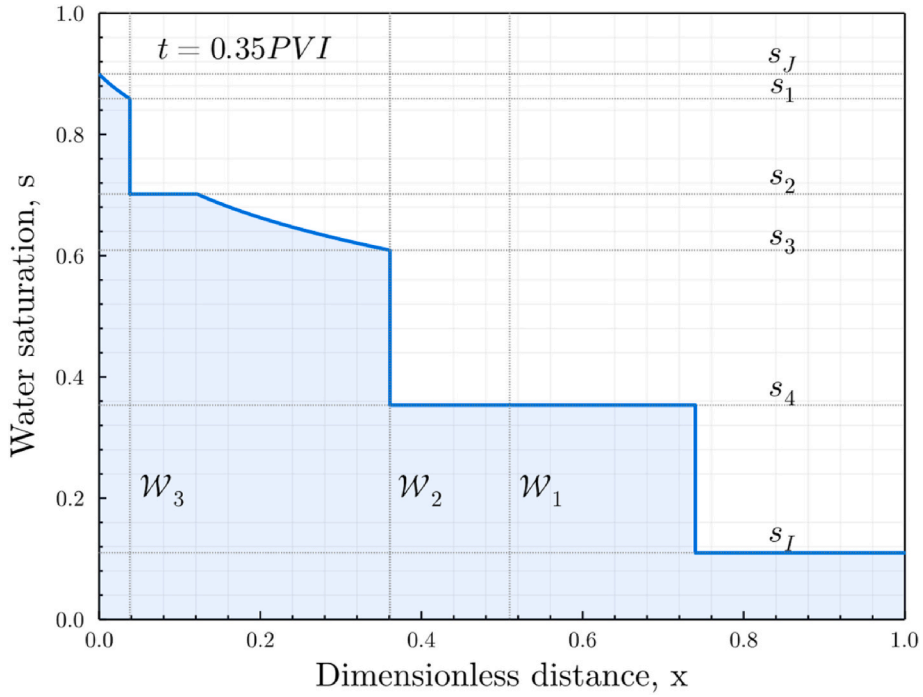

Fig. B.2. Water saturation profile for the solutions for SW-Gly5 injection at 0.35 PVI.

References

Abu-Al-Saud, M., Al-Ghamdi, A., Ayirala, S., Al-Otaibi, M., 2020. A surface complexation model of alkaline-SmartWater electrokinetic interactions in carbonates. Present. Int. Sympos. Soci. Core Analy. https://doi.org/10.1051/e3sconf/202014602003.

Al-Busaidi, I.K., Al-Maamari, R.S., Karimi, M., Naser, J., 2019. Effect of different polar organic compounds on wettability of calcite surfaces. J. Petrol. Sci. Eng. 180, 569–583. https://doi.org/10.1016/j.petrol.2019.05.080.

Al–Ibadi, H., Stephen, K.D., Mackay, E.J., 2019. Extended fractional-flow model of low-salinity waterflooding accounting for dispersion and effective salinity range. SPE J. 24 (6), 2874–2888. https://doi.org/10.2118/191222-PA.

Allan, J., Sun, S.Q., 2003. Controls on recovery factor in fractured reservoirs: lessons learned from 100 fractured fields. In: Presented at the SPE Annual Technical Conference and Exhibition. Denver, Colorado, USA, pp. 5–8. https://doi.org/10.2118/84590-MS. October. SPE-84590-MS.

Al-Sofi, A., Wang, J., AlBoqmi, A., AlOtaibi, M., Ayirala, S., Yousef, A.A., 2019. Smartwater synergy with chemical enhanced oil recovery: polymer effects on smartwater. SPE Reservoir Eval. Eng. 22 (1), 61–77. https://doi.org/10.2118/184163-PA. SPE-184163-PA.

Akbar, M., Vissapragada, B., Alghamdi, A.H., Allen, D., Herron, M., Carnegie, A., Dutta, D., Olesen, J.R., Chourasiya, R.D., Logan, D., Stief, D., 2000. A snapshot of carbonate reservoir evaluation. Oilfield Rev. 12 (4), 20–21.

Apolinário, F.D.O., Pires, A.P., 2021. Oil displacement by multicomponent slug injection: an analytical solution for Langmuir adsorption isotherm. J. Petrol. Sci. Eng. 197, 107939 https://doi.org/10.1016/j.petrol.2020.107939.

Awolayo, A.N., Sarma, H.K., 2019. An analytical solution to interpret active ion transport during chemically-tuned waterflooding process in high-temperature carbonate rocks. Can. J. Chem. Eng. 97 (1), 310–322. https://doi.org/10.1002/cjce.23183.

Bonto, M., Eftekhari, A.A., Nick, H.M., 2019. An overview of the oil-brine interfacial behavior and a new surface complexation model. Sci. Rep. 9 (1), 1–16. https://doi.org/10.1038/s41598-019-42505-2.

Borazjani, S., Behr, A., Genolet, L., Kowollik, P., Bedrikovetsky, P., 2019. Ion-exchange inverse problem for low-salinity coreflooding. Transport Porous Media 128 (2), 571–611. https://doi.org/10.1007/s11242-019-01260-8.

Borazjani, S., Dehdari, L., Bedrikovetsky, P., 2020. Exact solution for tertiary polymer flooding with polymer mechanical entrapment and adsorption. Transport Porous Media 134, 41–75. https://doi.org/10.1007/s11242-020-01436-7.

Brantson, E.T., Ju, B., Appau, P.O., Akwensi, P.H., Peprah, G.A., Liu, N., Aphu, E.S., Boah, E.A., Borsah, A.A., 2020. Development of hybrid low salinity water polymer flooding numerical reservoir simulator and smart proxy model for chemical enhanced oil recovery (CEOR). J. Petrol. Sci. Eng. 187, 106751 https://doi.org/10.1016/j.petrol.2019.106751.

Brady, P.V., Krumhansl, J.L., Mariner, P.E., 2012. Surface Complexation Modeling for Improved Oil Recovery. Presented Atthe SPE Improved Oil Recovery Symposium in Tulsa. Oklahoma, USA, pp. 14–18. https://doi.org/10.2118/153744-MS. April. SPE-153744-MS.

Chandrasekhar, S., Sharma, H., Mohanty, K.K., 2018. Dependence of wettability on brine composition in high temperature carbonate rocks. Fuel 225, 573–587. https://doi.org/10.1016/j.fuel.2018.03.176.

Clarke, R.G., Collins, C.M., Roberts, J.C., Trevani, L.N., Bartholomew, R.J., Tremaine, P. R., 2005. Ionization constants of aqueous amino acids at temperatures up to 250 C using hydrothermal pH indicators and UV-visible spectroscopy: Glycine, α-alanine, and proline. Geochem. Cosmochim. Acta 69 (12), 3029–3043. https://doi.org/10.1016/j.gca.2004.11.028.

Dzombak, D.A., Morel, F.M., 1990. Surface Complexation Modeling: Hydrous Ferric Oxide. John Wiley & Sons.

Ebrahim, T., Mohsen, V.S., Mahdi, S.M., Esmaeel, K.T., Saeb, A., 2019. Performance of low-salinity water flooding for enhanced oil recovery improved by SiO_2 nanoparticles. Petrol. Sci. 16, 357–365. https://doi.org/10.1007/s12182-018-0295-1.

Eftekhari, A.A., Thomsen, K., Stenby, E.H., Nick, H.M., 2017. Thermodynamic analysis of chalk–brine–oil interactions. Energy Fuel. 31 (11), 11773–11782. https://doi.org/10.1021/acs.energyfuels.7b02019.

Erzuah, S., Fjelde, I., Omekeh, A.V., 2019. Wettability estimation using surface-complexation simulations. SPE Reservoir Eval. Eng. 22 (2), 509–519. https://doi.org/10.2118/185767-PA. SPE-185767-PA.

Fathi, S.J., Austad, T., Strand, S., Puntervold, T., 2010. Wettability alteration in carbonates: the effect of water-soluble carboxylic acids in crude oil. Energy Fuel. 24 (5), 2974–2979. https://doi.org/10.1021/ef901527h.

Gbadamosi, A., Patil, S., Al Shehri, D., Kamal, M.S., Hussain, S.S., Al-Shalabi, E.W., Hassan, A.M., 2022. Recent advances on the application of low salinity waterflooding and chemical enhanced oil recovery. Energy Rep. 8, 9969–9996. https://doi.org/10.1016/j.egyr.2022.08.001.

Heberling, F., Trainor, T.P., Lützenkirchen, J., Eng, P., Denecke, M.A., Bosbach, D., 2011. Structure and reactivity of the calcite–water interface. J. Colloid Interface Sci. 354 (2), 843–857. https://doi.org/10.1016/j.jcis.2010.10.047.

Hiorth, A., Cathles, L.M., Madland, M.V., 2010. The impact of pore water chemistry on carbonate surface charge and oil wettability. Transport Porous Media 85 (1), 1–21. https://doi.org/10.1007/s11242-010-9543-6.

Hirasaki, G.J., 1991. Wettability: fundamentals and surface forces. SPE Form. Eval. 6 (2), 217–226. https://doi.org/10.2118/17367-PA.

Karimov, D., Hashmet, M.R., Pourafshary, P., 2020. A laboratory study to optimize ion composition for the hybrid low salinity water/polymer flooding. Present. Offshore Technol. Conf. Asia Malaysia 2–5. https://doi.org/10.4043/30136-MS. November. OTC-30136-MS.

Khorsandi, S., Qiao, C., Johns, R.T., 2017. Displacement efficiency for low-salinity polymer flooding including wettability alteration. SPE J. 22 (2), 417–430. https://doi.org/10.2118/179695-PA.

Khorsandi, S., Shen, W., Johns, R., 2016. Global riemann solver and front tracking approximation of three-component gas floods. Q. Appl. Math. 74 (4), 607–632. https://doi.org/10.1090/qam/1444.

Lake, L.W., Johns, R., Rossen, W.R., Pope, G.A., 2014. Fundamentals of Enhanced Oil Recovery, second ed. Society of Petroleum Engineers, Richardson, TX.

Lara Orozco, R.A., Abeykoon, G.A., Wang, M., Arguelles-Vivas, F., Okuno, R., Lake, L.W., Ayirala, S.C., AlSofi, A.M., 2020a. Amino acid as a novel wettability modifier for enhanced waterflooding in carbonate reservoirs. SPE Reservoir Eval. Eng. 23 (2), 741–757. https://doi.org/10.2118/195907-PA. SPE-195907-PA.

Lara Orozco, R.A., Abeykoon, G.A., Okuno, R., Lake, L.W., 2020b. An electro-kinetic study of amino acid and potential determining ions for enhanced waterflooding in carbonate reservoirs. SPE Reservoir Eval. Eng. 25 (2), 302–318. https://doi.org/10.2118/201482-PA. SPE-201482-PA.

Lara Orozco, R.A., Abeykoon, G.A., Okuno, R., Lake, L.W., 2021. The impact of Glycine on the zeta potential of calcite at different temperatures and brine compositions. Colloids Surf. A Physicochem. Eng. Asp. 624, 126851 https://doi.org/10.1016/j.colsurfa.2021.126851.

Manrique, E.J., Muci, V.E., Gurfinkel, M.E., 2007. EOR field experiences in carbonate reservoirs in the United States. SPE Reservoir Eval. Eng. 10 (6), 667–686. https://doi.org/10.2118/100063-PA. SPE-100063-PA.

Mohammadi, S., Kord, S., Moghadasi, J., 2019. The hybrid impact of modified low salinity water and anionic surfactant on oil expulsion from carbonate rocks: a dynamic approach. J. Mol. Liq. 281, 352–364. https://doi.org/10.1016/j.molliq.2019.02.092.

Moradi, S., Isari, A.A., Bachari, Z., Mahmoodi, H., 2019. Combination of a new natural surfactant and smart water injection for enhanced oil recovery in carbonate rock: synergic impacts of active ions and natural surfactant concentration. J. Petrol. Sci. Eng. 176, 1–10. https://doi.org/10.1016/j.petrol.2019.01.043.

Parkhurst, D.L., 1995. *User's Guide to PHREEQC: A Computer Program for Speciation, Reaction-Path, Advective-Transport, and Inverse Geochemical calculations*(No. 95-4227. US Department of the Interior, US Geological Survey.

Pires, A.P., Bedrikovetsky, P.G., Shapiro, A.A., 2006. A splitting technique for analytical modelling of two-phase multicomponent flow in porous media. J. Petrol. Sci. Eng. 51 (1–2), 54–67.

Pope, G.A., 1980. The application of fractional flow theory to enhanced oil recovery. SPE J. 20 (3), 191–205. https://doi.org/10.2118/7660-PA.

Qiao, C., Johns, R., Li, L., 2016. Modeling low-salinity waterflooding in chalk and limestone reservoirs. Energy Fuel. 30 (2), 884–895. https://doi.org/10.1021/acs.energyfuels.5b02456.

Sekerbayeva, A., Pourafshary, P., Hashmet, M.R., 2022. Application of anionic surfactant engineered water hybrid EOR in carbonate formations: an experimental analysis. Petroleum 8 (4), 466–475. https://doi.org/10.1016/j.petlm.2020.10.001.

Shakeel, M., Samanova, A., Pourafshary, P., Hashmet, M.R., 2021. Experimental analysis of oil displacement by hybrid engineered water/chemical EOR approach in carbonates. J. Petrol. Sci. Eng. 207, 109297 https://doi.org/10.1016/j.petrol.2021.109297.

Sharma, H., Mohanty, K.K., 2018. An experimental and modeling study to investigate brine-rock interactions during low salinity water flooding in carbonates. J. Petrol. Sci. Eng. 165, 1021–1039. https://doi.org/10.1016/j.petrol.2017.11.052.

Sharma, H., Mohanty, K.K., 2022. Modeling of low salinity waterflooding in carbonates: effect of rock wettability and organic acid distribution. J. Petrol. Sci. Eng. 208, 109624 https://doi.org/10.1016/j.petrol.2021.109624.

Taheriotaghsara, M., Bonto, M., Eftekhari, A.A., Nick, H.M., 2020. Prediction of oil breakthrough time in modified salinity water flooding in carbonate cores. Fuel 274, 117806.

Tessarolo, N., Wang, N., Wicking, C., Collins, I., Webb, K., Couves, J., Crouch, J., Durkan, C., Zeng, H., 2021. Identification of organic species with "double-sided tape" characteristics on the surface of carbonate reservoir rock. Fuel 288, 119627. https://doi.org/10.1016/j.fuel.2020.119627.

Tetteh, J.T., Alimoradi, S., Brady, P.V., Ghahfarokhi, R.B., 2020. Electrokinetics at calcite-rich limestone surface: understanding the role of ions in modified salinity waterflooding. J. Mol. Liq. 297 (1), 111868 https://doi.org/10.1016/j.molliq.2019.111868.

Tripathi, I., Mohanty, K.K., 2008. Instability due to wettability alteration in displacements through porous media. Chem. Eng. Sci. 63 (21), 5366–5374. https://doi.org/10.1016/j.ces.2008.07.022.

Van Cappellen, P., Charlet, L., Stumm, W., Wersin, P., 1993. A surface complexation model of the carbonate mineral-aqueous solution interface. Geochem. Cosmochim. Acta 57 (15), 3505–3518. https://doi.org/10.1016/0016-7037(93)90135-J.

Velasco-Lozano, M., Balhoff, M.T., 2021. A semi-analytical solution for countercurrent spontaneous imbibition in water-wet fractured reservoirs. Transport Porous Media 138, 77–97. https://doi.org/10.1007/s11242-021-01591-5.

Venkatraman, A., Hesse, M.A., Lake, L.W., Johns, R.T., 2014. Analytical solutions for flow in porous media with multicomponent cation exchange reactions. Water Resour. Res. 50 (7), 5831–5847. https://doi.org/10.1002/2013WR015091.

Yousef, A.A., Al-Saleh, S.H., Al-Kaabi, A., Al-Jawfi, M.S., 2011. Laboratory investigation of the impact of injection-water salinity and ionic content on oil recovery from carbonate reservoirs. SPE Reservoir Eval. Eng. 14 (5), 578–593. https://doi.org/10.2118/137634-PA. SPE-137634-PA.

Zhang, P., Austad, T., 2005. The relative effects of acid number and temperature on chalk wettability. Presented at the SPE international symposium on oilfield chemistry in the woodlands. Texas, USA, February 2. SPE-92999-MS. https://doi.org/10.2118/92999-MS.

Zhang, P., Tweheyo, M.T., Austad, T., 2007. Wettability alteration and improved oil recovery by spontaneous imbibition of seawater into chalk: impact of the potential determining ions Ca^{2+}, Mg^{2+}, and SO_4^{2-}. Colloids Surf. A: Physicochem. Eng. Aspect 301 (1–3), 199–208. https://doi.org/10.1016/j.colsurfa.2006.12.058.